Experimental validation of a prototype photonic Phase Optical Time Domain Reflectometer for SHM in large-scale infrastructures

Massimo Leonardo Filograno[1], George Piniotis[2], Vassilis Gikas[3], Vasileios Papavasileiou[4], Charis Gantes[5], Maria Kandyla[6], Christos Riziotis[7]

[1] National Hellenic Research Foundation, Theoretical and Physical Chemistry Institute, Athens 11635, Greece (filograno@eie.gr)
[2] National Technical University of Athens, School of Rural and Surveying Engineering, Zographos, 15780, Athens, Greece (piniotis@survey.ntua.gr)
[3] National Technical University of Athens, School of Rural and Surveying Engineering, Zographos, 15780, Athens, Greece (vgikas@central.ntua.gr)
[4] National Technical University of Athens, School of Civil Engineering, Zographos, 15780, Athens, Greece, (vdpapav@central.ntua.gr)
[5] National Technical University of Athens, School of Civil Engineering, Zographos, 15780, Athens, Greece, (chgantes@central.ntua.gr)
[6] National Hellenic Research Foundation, Theoretical and Physical Chemistry Institute, Athens 11635, Greece (kandyla@eie.gr)
[7] National Hellenic Research Foundation, Theoretical and Physical Chemistry Institute, Athens 11635, Greece (riziotis@eie.gr)

Keywords: *Phase-OTDR; Ground-based Microwave Interferometry; Fiber Bragg Gratings; Sensors; Structural Health Monitoring*

ABSTRACT

Extensive dynamic characterization and continuous Structural Health Monitoring (SHM) are crucial tools for reliable and safe operation of large infrastructures. This need is expected to accelerate in the near future, as the percentage of aging infrastructure is steadily increasing. In this work, we develop a minimally invasive and synchronous fiber optic monitoring prototype for SHM, based on Phase Optical Time Domain Reflectometry (Phase-OTDR), and we assess its applicability and performance to large-scale infrastructures, such as bridges. The study presents characterization tests on a scaled steel bridge, a laboratory model of a modular Bailey-type bridge of 1:2.5 scale. Experimental validation of the Phase-OTDR system is achieved by comparison with commercial monitoring systems, such as a Ground-Based Microwave Interferometer (GBMI), a laser tracker, and multipoint fiber-optic Bragg grating (FBG) strain transducers. Phase-OTDR systems have already demonstrated their value for SHM applications by revealing dynamic patterns as well as detecting and locating vibrations along the structure. Because the required complexity of these systems heavily limits their applicability, this study proposes efficient instrumentation with a balanced trade-off between performance and cost. The study includes the analysis of the effect of adjustable structural elements of the bridge, which enable damage simulation and tuning of its structural behavior. Finite-element modeling and simulations are employed to predict the bridge behavior and interpret the experimental measurements. The results of the study lead to useful conclusions regarding the applicability of the method to dynamic SHM.

I. INTRODUCTION

A. *Aging control of structures*

Civil structure maintenance is an expensive task, the importance of which is too often underestimated. Manual and periodic inspections of large structures, such as bridges, are crucial for proper maintenance. Such inspections are time-consuming and, if they are conducted through static and dynamic load tests, become particularly expensive while the structure remains unavailable to the public during tests. Therefore, dynamic, real-time, and constants inspection of civil structures is a highly desirable process, which can increase the structure availability and extend its lifetime, thanks to prompt maintenance operations.

Unfortunately, the number of structures, especially bridges, which need constant monitoring is increasing with time, and there are several cases of structures that reach collapse, sometimes with a long list of fatalities [Calvi]. Even collapsed structures need real-time, constant structural health monitoring (SHM) until complete demolition, to

prevent further fatalities. Currently, commercial technologies are not entirely suitable for this purpose. Typical SHM commercial sensors include strain gauges, accelerometers, geophones, inclinometers, displacement sensors, and seismic sensors. Some of these sensors are based on electrical transduction while others on optical interactions, such as optical fiber sensors.

Optical fiber sensors are smaller than their electrical counterparts. They can be wavelength multiplexed in order to combine several sensors on a single optical fiber, they are immune to Electro-Magnetic Interference (EMI), have wide bandwidths, and provide remote sensing thanks to low attenuation of optical fibers [Matias, Barrias]. Optical fiber sensors can be either point or distributed sensors. The latter can monitor several thousand points simultaneously, providing a significantly reduced cost per sensed point; however, depending on the specific technology and performance requirements, they can be particularly expensive overall. Typically, distributed optical fiber sensors are based on Rayleigh, Raman, or Brillouin scattering. The most suitable distributed technologies for real-time SHM of vibrations are based on Rayleigh and Brillouin scattering, while Raman-based sensors are commercially available for temperature monitoring [Lopez-Higuera, Barrias]. One sub-category of Rayleigh-based sensors is Phase-Optical Time-Domain Reflectometer (Phase-OTDR) systems, which are emerging as competitive distributed acoustic sensors [Zuyuan, Muanenda].

In this work, we present monitoring tests on a scaled steel bridge, a laboratory model of a modular Bailey-type bridge of 1:2.5 scale and 6.12 m length, undertaken with a home-built, cost-effective Phase-OTDR system, custom developed to meet the needs of SHM applications with affordable cost, compared against three commercial SHM sensors, *i.e.*, fiber Bragg gratings (FBGs), Ground-Based Microwave Interferometry (GBMI), and laser tracking. The crucial advantage provided by the Phase-OTDR system is the lower cost per sensed point, compared to the other point sensing technologies.

II. SETUP

A. *The scaled Bailey-type steel bridge*

Bailey bridges are through-type truss bridges, which are built on site from a pre-engineered system of ready-to-assemble components. The roadway is carried between two main girders, each of which is formed from panels with dimensions 3,0x1,5 m, pinned end-to-end. The different arrangements of panels are known as *trusses* and *storeys,* and there are seven types of Bailey bridge configurations, depending on the number of *trusses* and *storeys*. The scaled model in this study is based on a Bailey bridge 15,24 m long, single-truss and single-storey (one truss made of five panels and one storey at each girder) [DOA]. Figure 1 shows a schematic of the model bridge, which is 6.12 m long and is composed of five sections - bays of ~123 cm each.

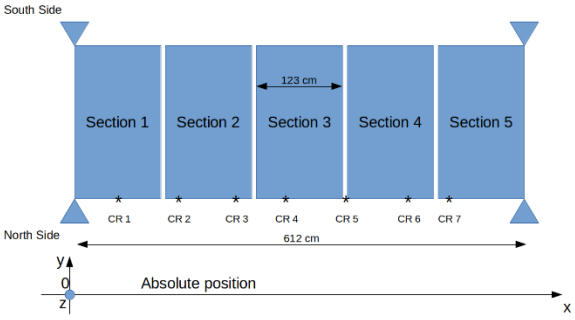

Figure 1: Schematic of the model bridge and corner reflector (CR) positions.

B. *The excitation source*

The excitation source utilized is a linear engine (shaker) that allows the generation of arbitrary waveforms. The apparatus used in the tests is the Modal 110 exciter of the company MB Dynamics Inc, and its main characteristics are as follows:

- Maximum Force: 500 N
- Bandwidth: DC-5000 Hz
- Max acceleration: 830 m/s^2 peak
- Max Velocity: 1.6 m/s peak
- Weight: 25 kg

The shaker is mounted with screws on the floor (Figure 2), and its position is fixed during all the tests. Its absolute position, according to the x-axis of Figure 1, is at 418.8 cm on the south side of the bridge.

Figure 2: Shaker apparatus setup.

A LabView application generated, in real-time, the incoming signals to the shaker, through a power

amplifier. The excitations provided to the bridge by the shaker are single harmonic, harmonic sweeps, shocks, and white noise excitations.

C. *Ground-Based Microwave Interferometry*

GBMI sensors are suitable for short period monitoring, due to their radiation exposure and visibility needs. The GBMI system used in this work is the IBIS-S (**I**mage **B**y **I**nterferometric **S**urvey of **S**tructures) system by the company IDS (Ingegneria Dei Sistemi, Pisa, Italy). This sensor implements two well-known radar techniques, *i.e.*, the Stepped-Frequency Continuous Wave technique, and the Interferometric technique, and allows displacement monitoring of several targets positioned at different distances from it, simultaneously [Gentile]. Since its first appearance in the SHM community, IBIS-S has been extensively used for dynamic testing of civil structures (*e.g.*, bridges, buildings, chimneys) and has become a well-established sensor for Non-Destructive Evaluation and Structural Health Monitoring. Figure 1 shows the corner reflectors (CR, targets) mounted on the north side of the bridge with the following absolute positions: 61 cm (CR1 in S1 – Section 1), 141 cm (CR2 in S2), 202 cm (CR3 in S2), 293 cm (CR4 in S3), 375 cm (CR5 between S3 and S4), 452.2 cm (CR6 in S4), 512 cm (CR7 in S5). Figure 3 shows a picture of the GBMI system and the seven CRs.

Figure 3. The GBMI system and the 7 CRs at the north side of the bridge.

D. *Photonic Sensors: FBGs and Phase-OTDR*

FBGs are narrow linewidth filters, the reflected wavelength of which depends on the strain and temperature changes applied to the filter. By introducing a broad spectrum in an FBG and monitoring the wavelength of the reflected signal, it is possible to retrieve the strain or temperature applied on the sensed point. FBGs are the optical equivalent of strain gauges, but they are intrinsically superior to the latter since FBG measurements are encoded in the wavelength of light and not in an amplitude signal, the performance of which is limited by noise. In this work, we used a commercial 4-channel FBG interrogator (MicronOptics sm130), which allows simultaneous monitoring of four optical fibers (each one with several FBGs available) at a maximum sampling rate of 1 kHz with a sensitivity of 1 με.

The Phase-OTDR systems use pulses of highly coherent light, introduced in a sensing optical fiber, to generate Rayleigh backscattering, a small light signal that is correlated to the state of the fiber. Any fiber change (due to strain and/or temperature) produces a change in the collected backscattered signal, which allows the localization of the perturbation and its spectral characteristics. Due to low-cost constraints, the Phase-OTDR system developed in this work cannot produce a linear relationship between the perturbation and the changes of the backscattered signal. Linearity for this kind of system is available only for very small perturbations. The system has a spatial resolution of 6 m. Therefore, it merges perturbations within this length. As it is shown later, this limitation, which becomes negligible for large structures, does not inhibit complete and useful structural analysis, since the system allows meaningful signal discrimination even within the resolution length.

As shown in Figure 4, there are 14 FBGs installed on the bridge, along with a continuous standard fiber for the Phase-OTDR system of 80 m, which senses the entire length of both sides of the bridge. The FBG locations are symmetric between the north and south sides, and their absolute locations are reported in

Table **1**. The FBG signals are converted to microstrain measurements. The continuous fiber is glued at the bottom of the base of the lower rods of the bridge both for the north and the south sides. The 68 m-long buffer coil of fiber (Figure 4) increases the degree of separation between the two bridge sides to avoid signal overlapping, generated by the 6-m resolution of the Phase-OTDR system.

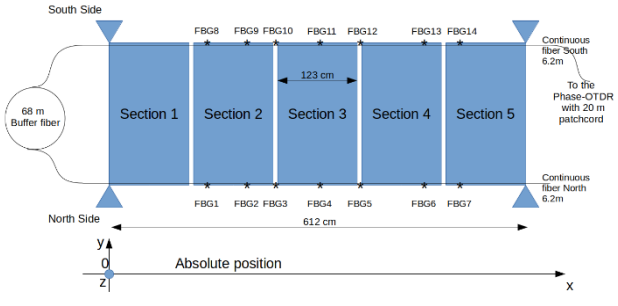

Figure 4: The 14 FBG point sensors locations and the continuous fiber, which senses both sides of the bridge.

Table 1: Absolute locations of FBGs.

FBG Number	Bridge Section	Position	Bridge Side	Absolute Position [cm]
1	2	up	North	152.8
2	2	up	North	202
3	2-3	down	North	245
4	3	up	North	307.5
5	4-5	down	North	368.4
6	4	up	North	460.2
7	5	up	North	512
8	2	up	South	152.8
9	2	up	South	202
10	2-3	down	South	245
11	3	up	South	307.5
12	4-5	down	South	368.4
13	4	up	South	460.2
14	5	up	South	512

FBGs are pasted at the bottom flange of the bottom chord of the bridge, either on the upper side of the flange (alongside the continuous fiber) or on the lower side. The second position is used for FBGs between two sections, which allows sensing the strain in the connecting element of two sections.

E. *The Laser Tracker system*

An additional monitoring system applied to the tests is the laser tracker (LT,

Figure **5**). The LT utilizes an extremely high-accuracy distance meter, which is combined with two angle encoders for measuring the elevation and rotational angles and permits the 3D position determination of a retroreflector that the tracker sensor is continuously tracking, thus allowing fast dynamic measurements.

Figure 5: The FARO Vantage laser tracker.

The laser tracker used in this work is the FARO Vantage model with the following characteristics:

- Distance accuracy: 16 µm + 0.8 µm/m
- Angular accuracy:20 µm + 5 µm/m
- Sampling rate: 1000 Hz max
- Range: 60 m max

The laser tracker calculates the x, y, and z displacements of a selected point on the bridge (axis orientation according to Figure 1). During the tests, were selected two such points on the south side of the bridge: a) one point at the absolute position of 411.2 cm (near the excitation shaker) and b) one point at 202.4 cm. The point at 411.2 cm allowed a reliable measure of the effective excitation provided to the bridge, while the point at 202.4 cm allowed the observation of the free movement of one bridge point with respect to the floor.

F. *Positioning of sensors*

The four types of sensors are located on the same sensing points on the bridge, to provide a correlation between signals. The FBGs share locations with the Phase-ODTR fiber. Two GBMI corner reflectors have two corresponding FBGs located very close (FBG2 = CR3, FBG7 = CR7). FBG9 and FB14 are located on the South side, symmetrically to the North-side FBG2 and FBG7. Finally, the laser tracker reflector was positioned during some tests near the excitation shaker rod and on others on a free-moving point.

III. THE FINITE-ELEMENT MODEL (FEM)

The FEM study was performed with the Sap2000 software. The recorded signal from the Laser Tracker was used as the input signal in the Load Cases of analysis. The analysis revealed that the 1st bending eigenfrequency (later called E_2, Figure 6) is very near to the experimental value, approximately 23.4 Hz. Similar results were found for the other eigenfrequencies as we show in the *Results and Discussion* section below.

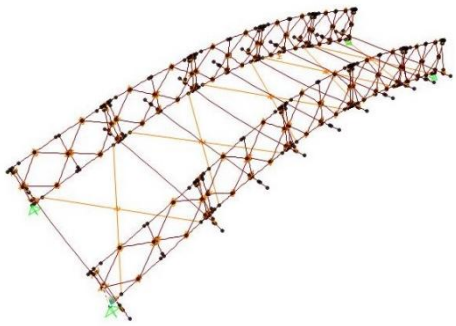

Figure 6: The first bending eigenfrequency, E_2, on the FEM simulation.

IV. RESULTS AND DISCUSSION

A. *Description of tests and preliminary observations*

We performed 18 tests, summarized in Table 2. The tests can be divided into four categories, depending on the excitation: a) single harmonic (1 Hz, 7.4 Hz, and 23 Hz), b) harmonic sweep (1-10 Hz and 5-50 Hz), c) shock, and d) white noise. The tests are also divided into two series; in the first series (tests 1 to 7) the LT is in position 1 (411.2 cm, near the excitation shaker) and the amplitude of the shaker excitation is lower; in the second series (tests 8-18) the LT is in the second position (202.4 cm), and the amplitude of the shaker excitation is higher. Repetition of some tests allows for repeatability check.

Table 2. Summary of applied tests.

Test number	Excitation type	LT position	Simulated Damage
1	1 Hz	Position 1	No
2	7.4 Hz	Position 1	No
3	23 Hz	Position 1	No
4	1-10 Hz Sweep	Position 1	No
5	5-50 Hz Sweep	Position 1	No
6	White Noise	Position 1	No
7	Shock	Position 1	No
8	1 Hz	Position 2	No
9	7.4 Hz	Position 2	No
10	23 Hz	Position 2	No
11	1-10 Hz Sweep	Position 2	No
12	5-50 Hz Sweep	Position 2	No
13	White Noise	Position 2	No
14	23 Hz	Position 2	No
15	White Noise	Position 2	No
16	White Noise	Position 2	Center North
17	White Noise	Position 2	Shaker South
18	23 Hz	Position 2	Shaker South

Figure 7-10 show the retrieved time response for test 9 for FBGs, Phase-OTDR, GBMI, and LT systems, respectively; the signals are plotted using an offset that allowed to keep all in a single figure. In Figure 7, the blue color is used for FBGs in the north side, while the red for the south side. The FBGs between sections (FBG3, FBG5, FBG10, and FBG12) collected a lower signal since they measure strain on a junction. The color pattern is the same for Figure 8 representing the Phase-OTDR signal retrieved for the position corresponding to the FBGs.

Table 3 summarizes the dominant frequencies in the signals collected in each test and by each technology: FBG, PO (Phase-OTDR), GBMI, LT. The tests are regrouped to compare those that share similar excitation signals. The dominant frequencies are directly identified in harmonic and shock tests while for white noise and sweep signals the determination is more complicated. Frequency values in bold are common for all the sensors of the same technology, while non-bold values are weak

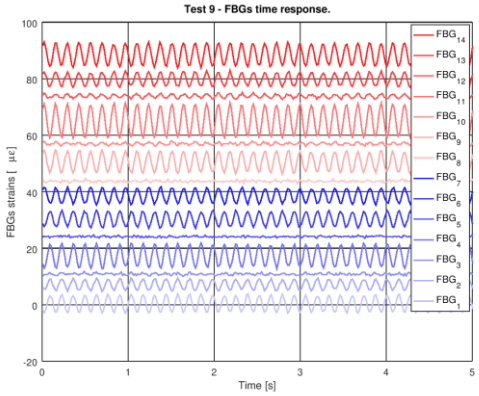

Figure 7: Time response of the 14 FBGs during test 9 (single harmonic 7.4 Hz).

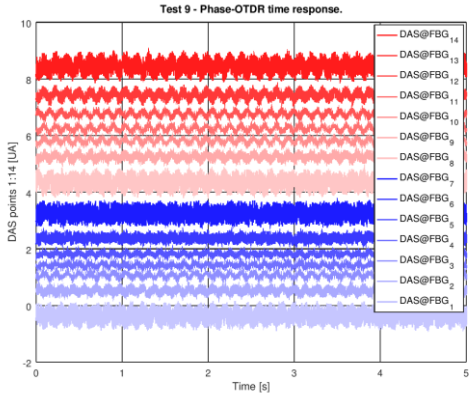

Figure 8: Time response of the Phase-OTDR system at the locations of the 14 FBGs.

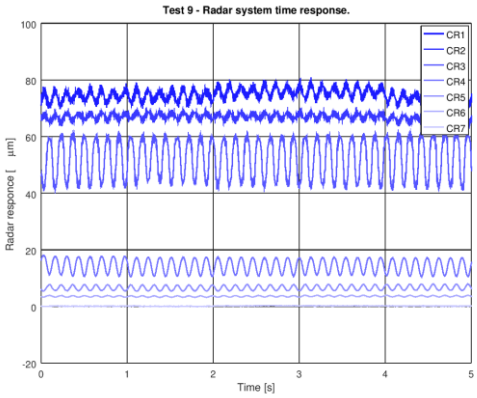

Figure 9: Time response of the GBMI corner CRs.

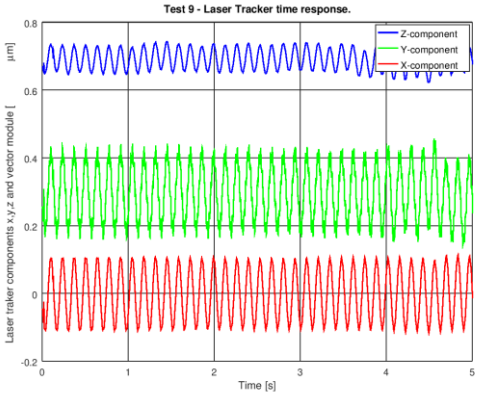

Figure 10: Time response of the LT.

and present in many but not all sensors. Frequency values in green correspond to the excitation frequencies and therefore are expected. Frequency values in red appear only for specific technologies and are related to the method used. GBMI often presents 50 and 25 Hz signals that could be related to cross-sensitivity of the system to power distribution lines in the laboratory room. The GBMI system also shows other "red" system-dependent frequencies: 90.6 Hz that is correlated to the CR rod support and 9.3-9.6 Hz sometimes revealed also by the LT. Since this last value appears for technologies that measure displacement from the floor but does not appear for technologies that measure deformations on the bridge, it is possible that this frequency is related to the support pillars of the bridge.

The single harmonic tests are chosen to study the behavior of the bridge at a low excitation frequency (1 Hz) and at the first two eigenfrequencies, E_1 and E_2, expected to be respectively at about 7.4 Hz and 23 Hz according to the eigenfrequencies computed by means of the FEM analysis.

As it is shown in Figure 7, sometimes time response signals appear weak, but even these signals carry enough spectral information for an SHM analysis. In Figure 11, we show the spectral analysis for a weak signal (FBG_9). The spectral analysis of such a weak signal, together with the input signal (7.4 Hz) and the 72 Hz mode, revealed the presence of the second eigenfrequency (E_2), while most of the other sensors were not able to do that.

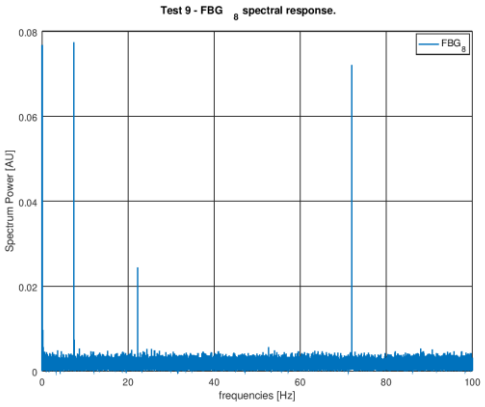

Figure 11: Spectrum response of a weak signal in test 9 (FBG_9).

Table 3. The dominant frequencies revealed by each technology: FBG, PO (Phase-OTDR), GBMI, LT.

Input type	Test #	Dominant Frequencies Revealed [Hz]
1 Hz	1	**FBG: 1, 72** **PO: 1, 72** **GBMI: 1, 9.5, 25, 50, 72, 90.6** **LT: 1**
		FBG: 1, 72
	8	**PO: 1, 72** **GBMI: 1, 9.5, 50,** 72, **90.6** **LT: 1, 51.6**
7.4 Hz	2	**FBG: 7.4,** 22.2, **72** **PO:** 1.62, **7.4, 72** **GBMI: 7.4, 9.4,** 22.2, 50, **90.6** **LT: 7.4,** 22.2
	9	**FBG: 7.4,** 22.2, **72** **PO: 7.4,** 22.2, **72** **GBMI: 7.4, 9.4, 50, 90.6** **LT: 7.4, 9.3**
23 Hz	3	**FBG: 23, 46,** 66, **69, 72,** 89, **92, 112, 115** **PO: 23, 46,** 66, **69, 72,** 89, **92, 112, 115** **GBMI: 9.4, 23, 46,** 50, **69, 90.6** **LT: 23, 46, 69**
	10	**FBG:** 7.7, 15.3, **23, 46, 69,** 72, **92, 112, 115** **PO:** 7.7, 15.3, **23, 46, 69, 72, 92, 112,** 115 **GBMI:** 7.7, **15.3, 23, 46,** 50, **69, 90.6** **LT:** 7.7, 15.3, **23,** 46, **69**
	14	**FBG:** 11.5, **23,** 34.5, **46,** 57.5, 66, **69,** 89, **92, 112, 115** **PO:** 11.5, **23, 34.5, 46,** 57.5, 66, **69,** 89, **92, 112,** 115 **GBMI:** 11.5, **23,** 34.5, 46, 90.6 **LT:** 11.5, **23, 46, 69**
	18	**FBG:** 20, **23, 46, 66, 69,** 72, **89, 92,** 112 **PO: 23, 46,** 66, **69,** 72, 89, 92, 112 **GBMI:** 9.4, 21.5, **23,** 46, **69, 90.6,** 92 **LT: 23, 46**
1-10 Hz Sweep	4	**FBG: 7.5,** 14.2, 16, 17.5, **20.5,** 72 **PO: 7.5,** 14.2, 16, 17.5, **20.5, 72** **GBMI: 7.5,** 17.5, **20.5, 25, 50, 90.6** **LT: 7.5, 16,** 17.5
	11	**FBG: 7.6,** 16, 17.5, **20.5, 72** **PO: 7.6,** 16, **17.5, 20.5, 72** **GBMI: 7.6,** 17.5, **20.5, 25, 50, 90.6** **LT: 7.6, 16,** 17.
5-50 Hz Sweep	5	**FBG:** 7.5, **20.5, 23, 25,** 91.2 **PO:** 7.5, **20.5, 23,** 91.2 **GBMI:** 7.5, **20.5, 23, 24,** 25, **50, 90.6** **LT: 7.5, 16, 20.5, 23**
	12	**FBG: 20.3,** 23 **PO: 20.3,** 23 **GBMI:** 7.5, **9.4, 20.3, 23,** 25, **44.7, 50,** 90.6 **LT: 7.5, 23**
White Noise	6	**FBG: 23, 24, 72** **PO:** 24, **72** **GBMI: 9.5, 25, 50, 90.6** **LT: 7.6, 9.5, 14.2 24**
	13	**FBG: 7.6, 23, 24, 72** **PO: 7.6, 23, 24, 72** **GBMI: 7.6, 9.4, 23, 24, 25, 50, 90.6** **LT: 7.6,** 24
	15	**FBG: 7.6, 20.3, 23, 24, 72** **PO: 20.3, 23, 24, 72** **GBMI: 7.6, 9.5, 20.3, 23, 24, 25, 50,** 81, **90.6** **LT: 7.6, 9.5, 23**
	16	**FBG: 7.6, 20.3, 23, 24, 72** **PO: 20.3, 23, 24, 72** **GBMI: 7.6, 9.5, 23, 24, 25, 50, 90.6** **LT: 7.6, 9.5, 14, 16, 23, 24**
	17	**FBG: 7.6, 20.3, 23, 24, 72** **PO: 20.3, 23, 24, 72** **GBMI: 7.6, 9.5, 23, 24, 25, 50, 90.6**

		LT: 7.6, 9.5, 14, 16, 23, 24
Shock	7	**FBG: 7.6, 72** **PO: 7.6, 72** **GBMI: 7.6,** 50**, 90.6** **LT: 7.6**

From Table 3 it is possible to deduce that in general the instrumented structure exalts preferably the eigenfrequency contained in the excitation source; *e.g.,* sweep tests tend to show E_1 and not E_2 when the sweep is between 1 and 10 Hz; while the presence of E_2 is stated clearly for sweep between 5 and 50 Hz. White noise input and, primarily, sweep input tests resulted in a significant number of harmonics present, some of which can be observed for all the sensors of the same technology, while others appear to be partially aleatory.

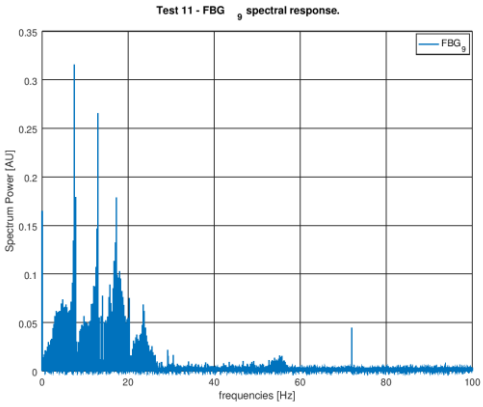

Figure 12: Spectral response of FBG_9 for the sweep input of test 11.

As it is shown in Figure 12, eigenfrequencies are spread due to the elements mismatch constituting the sections of the demountable structure. The effective eigenfrequencies E_1 and E_2 are respectively between 7.5 and 7.6 Hz and between 23 and 23.9 Hz.

FBGs and Phase-OTDR spectral analysis showed that E_2 values are higher (blue-shifted) on the side near the shaker (south side). This shift is possible due to the effect of the shaker or to a mismatch on the supports and the constitutive elements of the bridge. This peculiarity is not yet fully assessed. Test 7 (shock excitation) revealed the first eigenfrequency successfully, E_1, while it was not adequate to excite the second.

B. *Bridge fingerprinting and response to simulated damage*

Tests 16-18 are intended to show the bridge spectral response to two kinds of simulated damage, one severe damage at the center of the north side and one moderate damage near the shaker (south side). In an operating bridge, fingerprinting is obtained through the passing of a known vehicle or persons in pedestrian bridges. In the case of a laboratory test, a valid neutral and reproducible source is white noise. The wide bandwidth of this signal assures its neutrality. To study the effect of aging and wear, first, severe damage was simulated removing four bolts in a non-welded joining section in the north side of section 3 (see Figure 13), on the opposite side of the shaker (test 16).

Figure 13: The center joining section of the North side of section 3.

The second damage simulation (tests 17-18) was a smaller one, consisting of removing only one bolt on a similar joining section (the upper right screw of the center joining section). The second damage was simulated near the shaker (south side, section 4). Since the vibrational response of the bridge increases when the distance between damage and excitation source decreases, the second damage could appear as an unrealistic scenario. However, in any real scenario every bridge-crossing vehicle, sooner or later, passes near the damage, generating a peak in the magnitude of the retrieved data; such a peak corresponds to the second damage study. On the other hand, regarding sensor sensitivity, the first severe damage used for test 16 is a worst-case scenario for damage detection because it is relatively far from the excitation source. Indeed, the signals captured by the sensors are almost the same with and without the damage. Generally speaking, it is expected to have a signal increase if the bridge has greater mobility because of the reduced stability generated by damage and wear.

Figure 14-16 show the comparison of spectral analysis for tests 15 and 16 for FBG_{13}, the Phase-OTDR system at the location of FBG_{13}, and the CR_4, respectively, as examples of footprint change for the first damage. For these signals, the main changes are observed for the eigenfrequencies (E_2 and 72 Hz). E_2 is reduced in intensity and blue-shifted as a result of the damage, while the 72 Hz response is exalted.

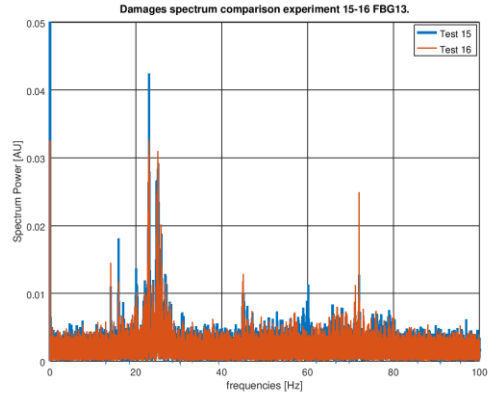

Figure 14: Footprint change due to the first damage (test 16 and reference test 15), revealed by FBG_{13}.

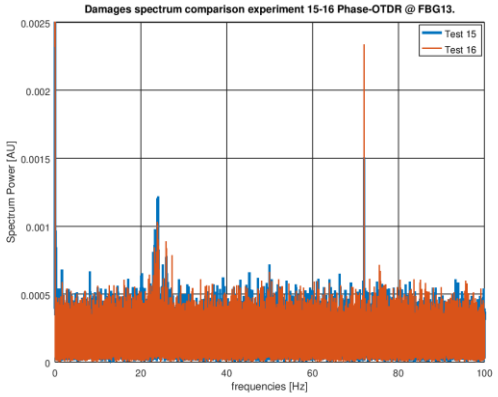

Figure 15: Footprint change due to the first damage (test 16 and reference test 15), revealed by the Phase-OTDR system at the location of FBG_{13}.

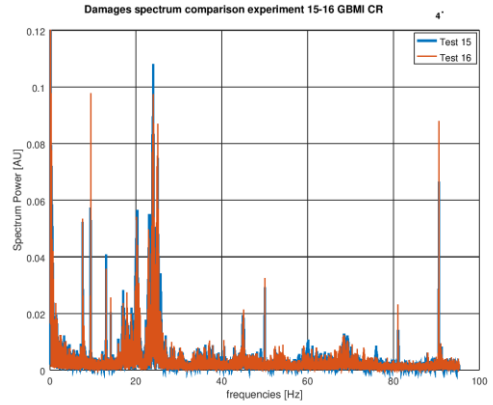

Figure 16: Footprint change due to the first damage (test 16 and reference test 15), revealed by CR_4.

It is possible to proceed with a similar analysis for all the sensors and other frequencies, *e.g.,* the frequency at 20.3 Hz, which changes in amplitude and shifts as a result of the damage. A stronger and error tolerant analysis can be performed using correlations between spectra. Due to the presence of eigenfrequencies around 23 Hz, this analysis can also be performed for the test of a single harmonic excitation.

As it is shown in Table 3, the spectral content in the retrieved signals changes slightly depending on the technology employed, but fundamental eigenfrequencies should be present in all sensing technologies since there is a common component (linearly related) for all the signal types (strain and displacement).

V. CONCLUSIONS

In this work, we showed four minimally invasive and synchronous monitoring techniques for SHM, and we assessed their performance on a scaled steel bridge, a laboratory model of a modular Bailey-type bridge of 1:2.5 scale. The experimental validation of the custom developed, low-cost Phase-OTDR system is achieved by implementing, in conjunction, commercial monitoring technologies, (FBGs, GBMI, and laser tracking). The results of the study prove the applicability of these methods to dynamic SHM, for safety and security purposes.

VI. ACKNOWLEDGMENTS

This project has received funding from the European Union Horizon 2020 research and innovation programme under the Marie Sklodowska-Curie grant agreement No 706221.

References

I. R. Matias, S. Ikezawa, J. Corres (2018). “Fiber Optic Sensors: Current Status and Future Possibilities” Smart Sensors, Measurement and Instrumentation; ISBN-10: 3319826212.

J. M. Lopez-Higuera, L. Rodriguez Cobo, A. Quintela Incera, A. Cobo, "Fiber Optic Sensors in Structural Health Monitoring," (2011). Journal of Lightwave Technology, vol. 29, no. 4, pp. 587-608, Feb.15, 2011. doi: 10.1109/JLT.2011.2106479

Gentile C. (2010). Application of Radar Technology to Deflection Measurement and Dynamic Testing of Bridges, Radar Technology, Guy Kouemou (Ed.), ISBN: 978-953-307-029-2, InTech

A. Barrias, J. R. Casas, S. Villalba (2016). “A Review of Distributed Optical Fiber Sensors for Civil Engineering Applications”, Sensors (Basel). 2016 May; 16(5): 748. Published online 2016 May 23. doi: 10.3390/s16050748

Y. Muanenda (2018). “Recent Advances in Distributed Acoustic Sensing Based on Phase-Sensitive Optical Time Domain Reflectometry”, Journal of Sensors, Volume 2018, Article ID 3897873, 16 pages, https://doi.org/10.1155/2018/3897873

H. Zuyuan, L. Qingwen, F. Xinyu, C. Dian, S. Wang, G. Yang (2018). “A Review on Advances in Fiber-optic Distributed Acoustic Sensors (DAS).“ Th2L.1. 10.1364/CLEOPR.2018.Th2L.1. Conference on Lasers and Electro-Optics/Pacific Rim.

G. M. Calvi, M. Moratti, G. J. O'Reilly, N. Scattarreggia, R. Monteiro, D. Malomo, P. M. Calvi, R. Pinho (2018). “Once upon a Time in Italy: The Tale of the Morandi Bridge”, Structural Engineering International, DOI: 10.1080/10168664.2018.1558033.

DOA - Department of the Army (1986). Bailey Bridges FM5-277, Washington D.C.